

Local measurements of turbulent angular momentum transport in circular Couette flow

M. J. Burin · E. Schartman · H. Ji

Received: 17 March 2009 / Revised: 18 September 2009 / Accepted: 24 September 2009 / Published online: 15 October 2009
© Springer-Verlag 2009

Abstract We report on velocity fluctuations and the fluctuation-driven radial transport of angular momentum in turbulent circular Couette flow. Our apparatus is short (cylinder height to gap width ratio $\Gamma \sim 2$) and of relatively high wall curvature (ratio of cylinder radii $\eta \sim 0.35$). Fluctuation levels and the mean specific angular momentum are found to be roughly constant over radius, in accordance with previous studies featuring narrower gaps. Synchronized dual beam Laser Doppler Velocimetry (2D LDV) is used to directly measure the $r - \theta$ Reynolds stress component as a function of Reynolds number (Re), revealing approximate scalings in the non-dimensional angular momentum transport that confirm previous measurements of torque in similar flows. 2D LDV further allows for a decomposition of the turbulent transport to assess the relative roles of fluctuation intensity and $r - \theta$ cross-correlation. We find that the increasing angular momentum transport with Re is due to intensifying absolute fluctuation levels accompanied by a slightly weakening cross-correlation.

1 Introduction

The study of fluid angular momentum transport between differentially rotating cylinders spans over a century, having originally begun with the torque studies of Couette (1890) and Mallock (1896). Taylor's landmark analysis (1923) established the viscous centrifugal instability criterion, along with the mathematical and physical character of the instability, which essentially takes the form of toroidal (a.k.a. Taylor) vortices. There are a host of interesting permutations and bifurcations of the Taylor vortex state that can exist at non-unique Reynolds numbers (e.g. Andereck et al. 1986). The Reynolds number (Re) is typically defined in this system as $Re \equiv \frac{\Omega_1 R_1 (R_2 - R_1)}{\nu}$, where $R_{1(2)}$ is the inner (outer) cylinder radius, Ω_1 the inner cylinder rotation rate, and ν the kinematic viscosity.

At sufficiently high Re , vortex dominated Taylor–Couette flow may yield to a state of featureless turbulence, as has been observed in high Re experiments (e.g. Smith and Townsend 1982). The Re at which this occurs is dependent upon a number of factors, including system curvature and flow history (hysteresis), but is typically $\geq 10^5$. Regardless of the exact state of the flow, however, a roughly constant value of angular momentum can be expected over most of the annular gap width, due to the fluid interior being well-mixed by vortices and/or turbulence, except for boundary layers near the cylinder walls. Largely flat radial profiles of angular momentum over radius have accordingly been observed in previous experiments (e.g. Taylor 1935). Furthermore, crossed hot-wire Reynolds stress measurements have demonstrated that the radial flux of angular momentum is also roughly constant over radius within the fluid interior (Smith and Townsend 1982). Recent simulations also reveal a relative constancy over radius of both mean angular

M. J. Burin (✉)
Department of Physics, California State University,
San Marcos, CA, USA
e-mail: mburin@csusm.edu

E. Schartman
Nova Photonics, Inc., One Oak Place,
Princeton, NJ 08540, USA

H. Ji
Plasma Physics Laboratory,
Princeton University, Princeton, NJ, USA

momentum and its turbulent radial flux (Bilson and Bremhorst 2007).

Angular momentum transport in TC flows is typically observed as a torque upon the inner and/or outer cylinder. From the azimuthal component of the momentum balance, this torque is seen to be

$$\tau = 2\pi \left(\rho r^2 \langle v_r v_\theta \rangle - \nu \rho r^3 \frac{\partial}{\partial r} \left(\frac{V_\theta}{r} \right) \right), \quad (1)$$

where τ is the measured torque per unit length, ρ is the fluid density, and the bracketed quantity represents the time-averaged $r - \theta$ Reynolds stress component (v_j being a velocity fluctuation). Here, the first term represents advection due to fluctuations and the second term viscous diffusion. To compare with earlier studies featuring torque measurements, the measured velocity correlation is discussed here as a dimensionless torque per unit length, G , which (neglecting the viscous term) is

$$G \equiv \frac{2\pi r^2 \langle v_\theta v_r \rangle}{\nu^2}. \quad (2)$$

In torque measurements, G is typically given as

$$G \equiv \frac{2\pi\tau}{\rho\nu^2}. \quad (3)$$

Power-law scaling relations are sought of the form $G \propto Re^\alpha$. For a purely laminar viscous flow $\alpha = 1$, a fact utilized in viscometers, while for a vortex-dominated flow, the scaling exponent can be expected, according to some formulations, to be either 3/2 or 5/3 (Donnelly and Simon 1960; Barcion and Brindley 1984). In principle α cannot exceed 2, which is a fundamental asymptotic limit imposed by the Navier–Stokes equations (Doering and Constantin 1992). In experimental studies of high Re circular Couette flows, it has been observed that α can exceed 5/3. It is typically found to be around 1.7–1.8 for flows with Re of the order 10^5 – 10^6 (Wendt 1933; Taylor 1936; Barcion and Brindley 1984; Tong et al. 1990; Racina and Kind 2006).

From the most precise torque datasets, it can be concluded that a pure scaling law does not in fact exist: α is observed to be a monotonically increasing function of Re (Lathrop et al. 1992a, b; Lewis and Swinney 1999). Theoretical progress has recently been made which explains this trend by Eckhardt et al. (2007), who extend the well-known analogy of Taylor–Couette flow with Rayleigh–Bérnard convection to argue that α should be between 3/2 and 2, where the lower bound represents transport dominated by boundary layers, and increasing values beyond it indicate the increasing role of turbulent fluctuations within the fluid interior. Boundary layer theory can provide an alternate explanation of the torque scaling behavior (Panton 1992). Defining a skin friction coefficient to be

$C_f = G/Re^2$, logarithmic scaling of C_f is observed and the value of α can be accurately predicted (Lewis and Swinney 1999).

2 Experimental details

2.1 Apparatus

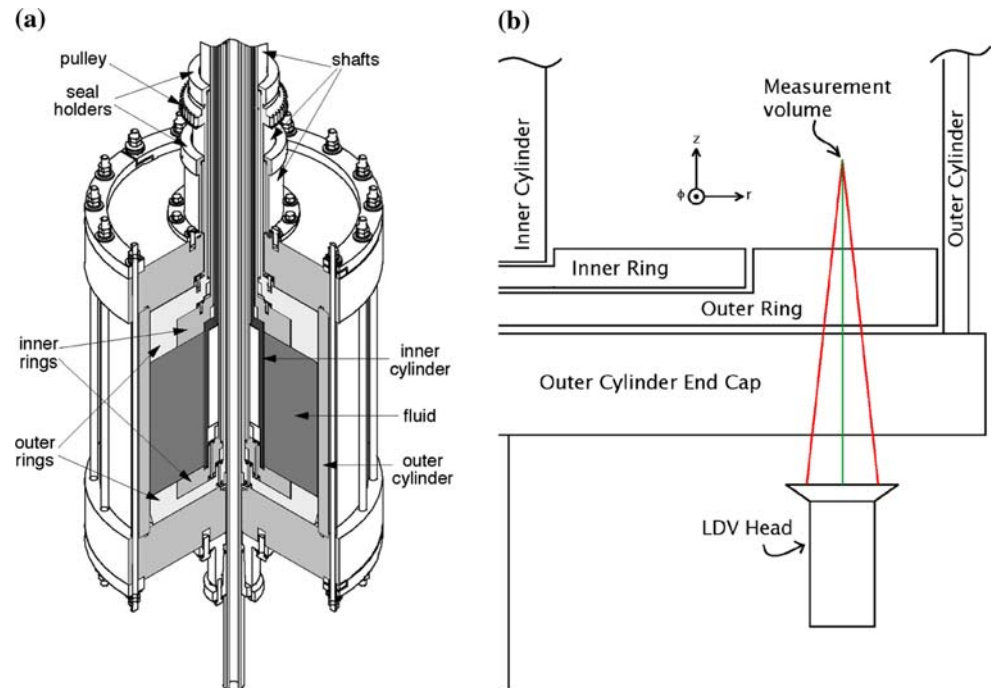
A schematic of our experimental apparatus is given in Fig. 1a. Note that we have modified the traditional circular Couette design to include two independent end-rings between the inner and outer cylinders, allowing for step-wise differential rotation at the vertical boundaries, as was proposed in Kageyama et al. (2004). These rings allow for a significant reduction of friction-driven secondary flows (Ekman circulation). We are thus able to create a Couette-like velocity profile, i.e. the ideal profile for diminishing gap width (or frictionless end-caps), in a wide-gap apparatus. For more detailed information on the apparatus and its operation, see Burin et al. (2006) and Schartman et al. (2009).

The experiments reported here were performed with water and a water/glycerol mixture (with $v_{\text{mix}} \approx 18\nu_{\text{H}_2\text{O}}$, $\rho_{\text{mix}} \approx 1.2\rho_{\text{H}_2\text{O}}$) at room temperature. The turbulence was driven in most cases by running the apparatus in a ‘split’ configuration, i.e. with the inner cylinder and inner ring at some finite speed, and the outer cylinder and outer ring held stationary in the lab frame. Turbulence was also generated with boundary conditions different from these to investigate the generality of our results. These preliminary studies have revealed that the exact driving mechanism of the turbulence is not important (see caption Fig. 4). The Reynolds number was varied by changing the speed of the inner two components of the device. We allowed for sufficient time to pass (3–5 min) after varying component speeds to allow for equilibration (i.e. spin-up/down) of the new flow state (Schartman et al. 2009). The steadiness of the new flow state was then confirmed by the convergence of statistical measures of interest.

2.2 Data acquisition

Our data was obtained via Laser Doppler Velocimetry (LDV), a well-known technique yielding time-series of velocity data $V_i(t)$ from which various statistics may be estimated. Radial profiles of azimuthal (θ , i.e. circumferential) velocity $V_\theta(t)$ were measured from the side of the apparatus. To measure correlated fluctuations ($\langle v_\theta v_r \rangle$, where $v_i = V_i - \langle V_i \rangle$), we utilized two synchronized orthogonal LDV beam pairs from underneath the apparatus, so that the radial and azimuthal components of velocity could be measured simultaneously. This technique can

Fig. 1 **a** Apparatus detail. Inner cylinder radius is 7.1 cm, outer cylinder 20.3 cm. Cylinder heights are 28.0 cm, giving an aspect ratio Γ of ~ 2 and a radius ratio $\eta \sim 0.35$. **b** Arrangement for 2D LDV data acquisition. Note the beam pair measuring azimuthal velocity is orthogonal to the plane of the paper and so appear as one in the figure



ultimately yield a time-series of the correlation $\langle v_\theta v_r \rangle$. A sketch of the experimental arrangement including the LDV diagnostic is shown in Fig. 1b.

The 2D LDV method here employed is complementary to the aforementioned torque method. It also has an advantage over torque measurement by being a *local* and *direct* measurement, and an advantage over in situ probes by being unpeturbative to the fluid. Though LDV has been used to study Reynolds stress components in other rotating flow configurations (e.g. Marie and Daviaud 2004), our work (here and in Ji et al. 2006; Burin et al. 2008) is apparently the first application of 2D LDV to circular Couette flow. Note that there are two practical requirements for applying 2D LDV to circular Couette flow that have enabled our measurements: to be able to observe the fluctuation correlation pair $\langle v_\theta v_r \rangle$ needed for angular momentum transport, one needs transparent end-caps (to access the fluid vertically), and a relatively wide gap between cylinders (to allow for the width of the incoming beam pair).

3 Analysis and discussion

3.1 On the lack of vortex structure

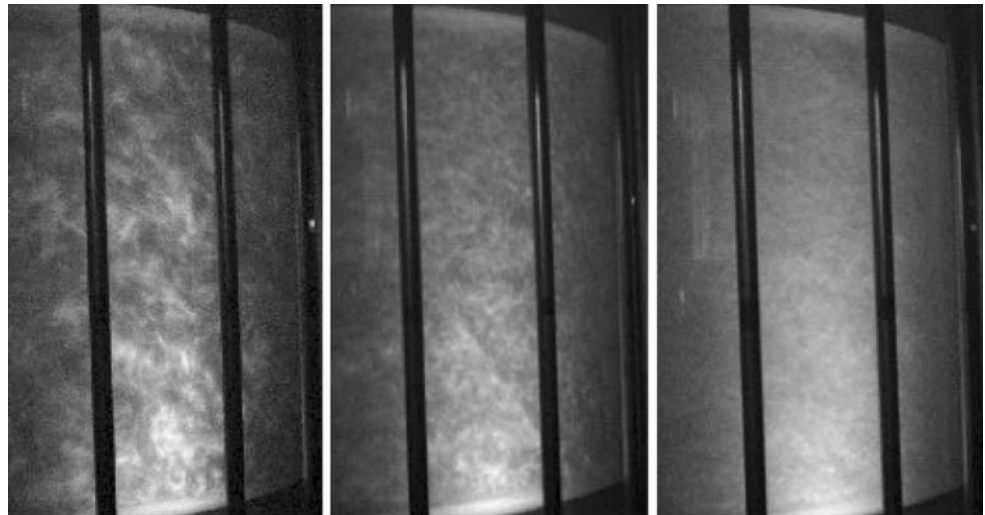
Our velocity data (both mean and fluctuating) lack significant variations in z within the bulk of the fluid, indicating that there is insignificant Taylor vortex structure, in agreement with other high Re (order of 10^5 – 10^6)

experiments (Smith and Townsend 1982; Lewis and Swinney 1999), as well as qualitative imaging of the flow: example photographs using KalliroscopeTM at three characteristic Re can be seen in Fig. 2, where both the lack of vortex structure and decreasing eddy length scale with Re are apparent. In a short aspect ratio device, such as ours ($\Gamma = 2$), one should expect a low number of cells (two, or perhaps even one; e.g. Lücke et al. 1984; Koga and Koschmieder 1989). Since our lowest Re is approximately 20 times the critical Re for vortex onset (according to the formulation by Roberts 1965), these cell(s) could be fairly distorted and/or recessed from the outer cylinder. These factors inhibit the visual discernment of axial structure within the flow if it is present.

3.2 Mean radial profiles

Figure 3 presents radial profiles of azimuthal velocity and specific angular momentum for four characteristic rotation speeds. These are given at a height of 7.1 ± 0.2 cm from the lower surface, corresponding to $\frac{1}{4} H$. The velocity profiles of water and the glycerol mix (Fig. 3a) are nearly identical, and profiles at other heights (not shown) also look indistinguishable, except for very close to the boundary ($< \frac{1}{2}$ cm; note the viscous Ekman layer thickness is expected to be at most 2 mm, and is typically well under 1 mm). We note that at $r = 8.5$ cm (approximately 1.5 cm from the inner cylinder surface) the speed has already dropped to roughly half of the inner cylinder speed. Difficulties from reflections and diagnostic positioning prevent

Fig. 2 Photographs of the fluid with KalliroscopeTM for Re of approximately 10^4 , 5×10^4 , and 2×10^5 , respectively (from left). The fluid is illuminated from below. A lack of vortex structure and decreasing eddy length scale are apparent. Note that the vertical dark bars are tie-rods on the apparatus



us from observing the steep velocity gradient near the inner cylinder surface.

For the angular momentum of the bulk flow, when the outer cylinder is stationary, a value of half of the angular momentum of the inner cylinder may be expected (Taylor 1935; Smith and Townsend 1982). In Fig. 3b, we observe that the average specific angular momentum is somewhat more than this value. This is due to an additional torque from the inner ring, which rotates at the same rate as the inner cylinder, but at a larger mean radius. We also note that the four average momenta scale well. That is, they are all nearly at the same magnitude relative to the angular momentum of the inner cylinder.

The error bars in Fig. 3 are fluctuation RMS values, which can be physically interpreted as the level of turbulence intensity. Turbulence levels for both $V_r(t)$ and $V_\theta(t)$ are roughly constant over radius within the bulk of the

fluid, consistent with earlier experimental studies (Smith and Townsend 1982) and high Re simulations (Bilson and Bremhorst 2007; Dong 2007). Fluctuation amplitudes as a function of Re are discussed below.

3.3 Turbulent angular momentum transport

Figure 4 displays the scaling of non-dimensional angular momentum transport (G) with Re for the turbulent flow. There is at first glance a single slope (α) over the entire Re range; a fit yields $\alpha = 1.65 \pm 0.05$. Fitting the data for each fluid Re range individually, however, reveals that the derived scaling exponents could be considered to be statistically distinct: $G \propto Re^{1.60 \pm 0.10}$ for $2 \times 10^3 < Re < 1 \times 10^4$ (with glycerol mix) and $G \propto Re^{1.77 \pm 0.07}$ for $2 \times 10^4 < Re < 2 \times 10^5$ (with water). Errors here represent the standard error of a log–log linear fit; they do not include

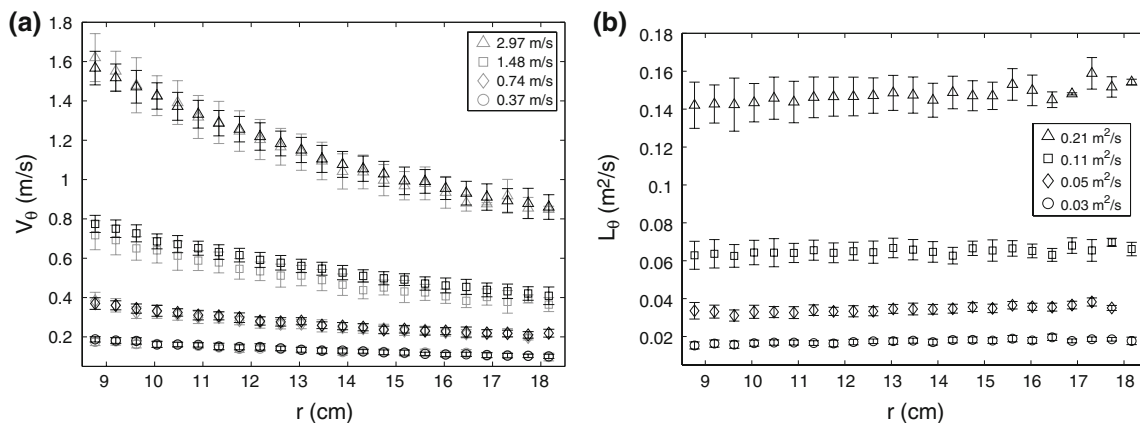


Fig. 3 Mean azimuthal velocity (a) and specific angular momentum (b) for four characteristic inner cylinder (and inner ring) speeds, corresponding to Reynolds numbers of approximately 5×10^4 , 1×10^5 , 2×10^5 , and 4×10^5 . Values in the legends represent the

rotational surface speed (a) and specific angular momentum of the inner cylinder surface (b). The velocities from both water and the glycerol mix are overlaid in (a); water in black and the glycerol mixture in gray. All data are from $z = 7$ cm

slight measured variations in fluid temperature ($22 \pm 2^\circ\text{C}$) that affect viscosity, especially that of the glycerol mixture (Shankar and Kumar 1994). The data were obtained in varied time sequences, however (i.e. fluid heating and prescribed flow speed are uncorrelated), so while viscosity variations due to temperature may add to the inherent scatter, they should not in principle affect the inferred scaling exponents. The observed values of α between 1.6 and 1.8 confirm the previous aforementioned measurements utilizing torque at high Reynolds numbers. However, since the distinctness of the two slopes is only at the 1σ level, more data is needed to clarify the exact value and trend of the slope(s) with respect to Re .

Each datapoint in Fig. 4 typically represents a dataset of 1,000 points. Unfortunately, we are limited in data-rate due to the large acrylic end-caps imaged through (approximately 16.25 cm thick), and are also limited in total collection time due to heating concerns. Nonetheless, given this level of accuracy, it does appear that α increases slightly with Re , as observed in previous work (Barcilon and Brindley 1984; Lathrop et al. 1992a, b; Lewis and Swinney 1999). Given this observation, we have reformulated the $\langle v_\theta v_r \rangle$ correlation data in terms of a skin friction coefficient $C_f = G/Re^2$ in order to compare with boundary layer theory, with the results seen in Fig. 5. The log-law fit appears valid and yields a slope of 1.40 ± 0.16 , which is within a standard error of the values derived from

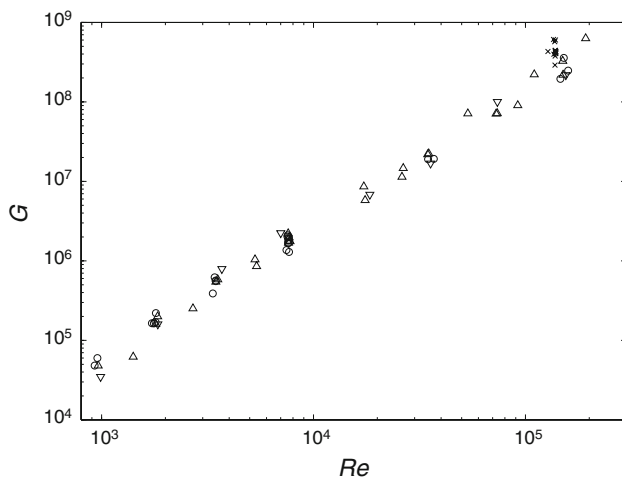


Fig. 4 Reynolds number scaling of non-dimensional angular momentum transport G . The break near $Re = 10^4$ is in-between fluid types. Triangles represent data for Re increasing, inverted triangles for Re decreasing. Data are from $r = 17$ cm, $z = 7$ cm, except for circles, which represent data from various other locations within the fluid interior; typically 1–3 cm away from 17 cm in r and/or up to 6 cm away in z (i.e. down to $z = 1$ cm). The crosses (x) near $Re = 1.5 \times 10^5$ are from data obtained with a different driving scheme (i.e. not ‘split’), also at various interior locations

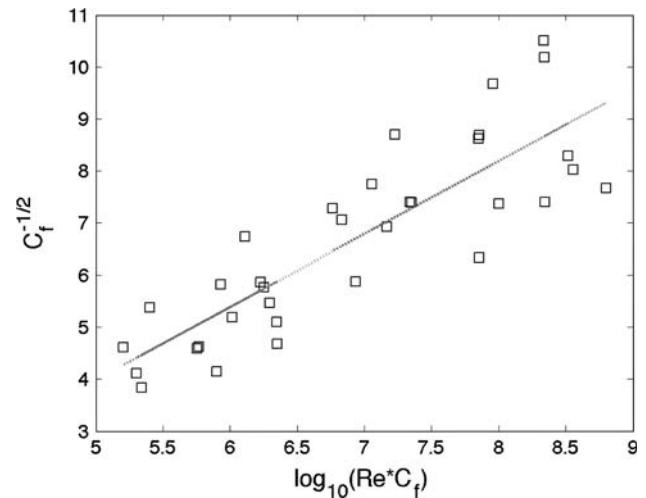


Fig. 5 Logarithmic scaling from the wall friction formulation, yielding a slope of 1.40 ± 0.16 . Data are the same as in Fig. 4

previous torque results (1.52 in Lathrop et al. 1992a, b and 1.56 in Lewis and Swinney 1999).

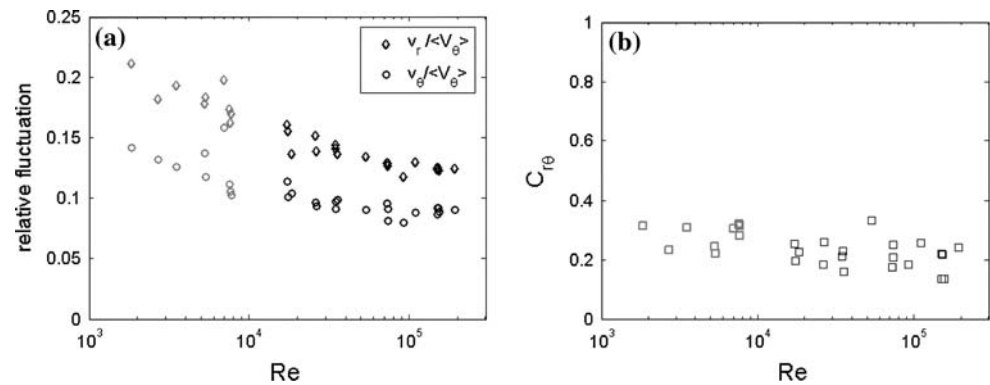
Although additional data is needed for a more precise determination of these fits (both power-law and logarithmic), the current data clearly demonstrates the promise of 2D-LDV as a useful alternate diagnostic. We note that the data have been compiled from independent data sets to demonstrate repeatability of the results. The data were also studied for hysteresis effects, which are evidently absent (see Fig. 4 caption). The results are independent of location within the fluid interior, and also appear to be independent of the driving scheme behind the turbulence.

3.4 Trends in fluctuation intensity and cross-correlation

Though the RMS of the fluctuations increase with the mean flow speed, the relative fluctuations (normalized by the mean flow speed) are observed to slightly decrease with Re , as seen in Fig. 6a. Radial fluctuations are consistently more intense by a factor $\leq 50\%$, consistent with earlier experimental findings (Smith and Townsend 1982; Lewis and Swinney 1999). Over the entire Re range both fluctuation quantities may be roughly described as decaying like $\frac{\langle v \rangle_{RMS}}{\langle V \rangle} \propto Re^{-0.11}$. This exponent is close to the one found by Lewis and Swinney (1999), who obtained -0.125 for the relative azimuthal fluctuations. But the overall power-law fit for our data is rather poor, except for radial fluctuations above $Re = 10^4$. Nonetheless a fluctuation decay exponent of -0.11 does provide a rough consistency check to our results in view of the scaling of G in the asymptotic limit (where $\alpha = 2$), since $Re^{2-2(0.11)} = Re^{1.78}$.

A further advantage of the 2D LDV technique is that one may decompose the components that comprise G ,

Fig. 6 Reynolds number versus **a** relative fluctuation intensities and **b** their cross correlation coefficient. All data are from $r = 17$ cm, $z = 7$ cm



understanding that the $r - \theta$ Reynolds stress component can be seen as

$$\langle v_r v_{\theta} \rangle = \langle v_r \rangle_{\text{RMS}} \langle v_{\theta} \rangle_{\text{RMS}} C_{r\theta}, \quad \text{where } C_{r\theta} \equiv \frac{\langle v_{\theta} v_r \rangle}{\langle v_{\theta} \rangle_{\text{RMS}} \langle v_r \rangle_{\text{RMS}}} \quad (4)$$

$C_{r\theta}$ is given as a function of Re in Fig. 6b, where a slight but certain decrease with Re can be seen. From this, we may conclude that the observed increase in fluctuation-driven angular momentum transport is solely due to increasing (absolute) fluctuation intensity, and not due to any increased correlation between azimuthal and radial velocity fluctuations. The decreasing cross-correlation coefficient with Re can simply be understood to be a result of the flow becoming increasingly random. We may compare $C_{r\theta}$ from our data with a value inferred from previous hotwire work at a similar Re . Near $Re = 50,000$ it is observed in Smith and Townsend (1982) that $C_{r\theta} \sim 30\text{--}40\%$ at a similar non-dimensional radius as our measurements, whereas we have $C_{r\theta} \sim 20\%$. The higher published value is perhaps due to some remnant vortex structure in the flowfield. Unfortunately, no other high Re correlation measurements from circular Couette flow appear to be available in the literature for comparison.

With increasing turbulence intensity, the role of intermittency is perhaps of import. That is, the significance of any trends in the velocity distribution tails should be assessed. Towards this end, we have examined the flatness factor as a function of Re for v_{θ} , v_r , $\langle v_{\theta} v_r \rangle$, and have found nothing of significance—flatness values are observed to stay roughly constant with Re . Thus, intermittency does not affect the scaling of the angular momentum transport.

3.5 Closing comments; geometrical issues

The similarity of our results to previous torque measurements, in conjunction with the relatively novel geometry of our apparatus, warrants some additional comments. First, in having a shorter aspect ratio, one might expect our results to differ more significantly from other studies due to boundary (Ekman) flows. But since the flow is strongly

unstable, Ekman pumping is relatively unimportant to the fluid interior, so the relative proximity of the vertical boundaries is of little consequence in this regard. This result is perhaps foreshadowed in Lewis and Swinney (1999), who found no difference in the scaling of G between $\Gamma = 9.8$ and 11.4 . Results from Cole (1976) are likewise similar. More relevant to our geometry are the measurements of Tong et al. (1990), who found a similar exponent ($\alpha = 1.8$) in a $\Gamma < 2$ device.

Lastly, we consider the issue of wall curvature, typically characterized by the radius ratio $\eta \equiv r_1/r_2$, or the non-dimensional gap width $1 - \eta$. It is well known that curvature affects Taylor vortex dynamics, e.g. the critical Re (as reflected in the Taylor number) as well as details of the instability bifurcation sequence. Curvature conceivably affects turbulent angular momentum transport as well, although to date there is only sparse data on this issue for wider gap widths. Experimental work has found, however, that while the magnitude of the transport (G) depends on curvature (η), the scaling exponent (α) does not (e.g. Racina and Kind 2006). This conclusion is shared by theory (Eckhardt et al. 2007). In this light, then, it is not surprising that our (wide-gap, LDV-based) exponents are consistent with previous (narrow-gap, torque-based) results. That the magnitude of the transport we observe (e.g. $G \sim 10^8$ at $Re \sim 10^5$) roughly agrees with previous work of different geometry is perhaps more curious; but even so, the proposed theoretical dependence on η is minor except in the limit $\eta \rightarrow 1$, i.e. for very narrow gaps, as in journal bearings. For wider gaps, the magnitude of G should be less sensitive to η (Donnelly and Simon 1960; Bilgen and Boulos 1973).

Acknowledgement The LDV system used in this work was leased from Dantec Dynamics, Inc.

References

- Andereck CD, Liu SS, Swinney HL (1986) Flow regimes in a circular Couette system with independently rotating cylinders. *J Fluid Mech* 164:155

- Barcion A, Brindley J (1984) Organized structures in turbulent Taylor–Couette flow. *J Fluid Mech* 143:429 (data by F. R. Mobbs)
- Bilgen E, Boulos R (1973) Functional dependence of torque coefficient of coaxial cylinders on gap width and Reynolds numbers. *Trans ASME J Fluids Eng* 95:122
- Bilson M, Bremhorst K (2007) Direct numerical simulation of turbulent Taylor–Couette flow. *J Fluid Mech* 579:227
- Burin MJ et al (2006) Reduction of Ekman circulation in Taylor–Couette flow. *Exp Fluids* 40:962
- Burin MJ, Schartman E, Ji H (2008) Studies of turbulent angular momentum transport in Taylor–Couette flow via 2D laser doppler velocimetry. *J Phys Conf Ser* 137:012020
- Cole JA (1976) Taylor-vortex instability and annulus length effects. *J Fluid Mech* 75:1
- Couette M (1890) Etude sur le frottement des liquides. *Ann Chim Phys* 21:433
- Doering CR, Constantin P (1992) Energy dissipation in shear driven turbulence. *Phys Rev Lett* 69:1648
- Dong S (2007) Direct numerical simulation of turbulent Taylor–Couette flow. *J Fluid Mech* 587:373
- Donnelly RJ, Simon NJ (1960) An empirical torque relation for supercritical flow between rotating cylinders. *J Fluid Mech* 7:26 with an appendix by Batchelor G
- Eckhardt B, Grossman S, Lohse D (2007) Torque scaling in turbulent Taylor–Couette flow between independently rotating cylinders. *J Fluid Mech* 581:221
- Ji H, Burin MJ, Schartman E, Goodman J (2006) Hydrodynamic turbulence cannot transport angular momentum effectively in astrophysical disks. *Nature* 444:343
- Kageyama A et al (2004) Numerical and experimental investigation of circulation in short cylinders. *J Phys Soc Jpn* 73:2424
- Koga JK, Koschmieder EL (1989) Taylor vortices in short fluid columns. *Phys Fluids A* 1:1475
- Lathrop D, Fineberg J, Swinney HL (1992a) Transition to shear-driven turbulence in Taylor–Couette flow. *Phys Rev A* 46:6390
- Lathrop D, Fineberg J, Swinney HL (1992b) Turbulent flow between concentric rotating cylinders at large Reynolds number. *Phys Rev Lett* 68:1515
- Lewis GS, Swinney HL (1999) Velocity structure functions, scaling, and transitions in high-Reynolds-number Couette–Taylor flow. *Phys Rev E* 59:5457
- Lücke M, Mihelcic M, Wingerath K, Pfister G (1984) Flow in a small annulus between concentric cylinders. *J Fluid Mech* 140:343
- Mallock A (1896) Experiments on fluid viscosity. *Phil Trans R Soc Lond A* 187:41
- Marie L, Daviaud F (2004) Experimental measurement of the scale-by-scale momentum transport budget in a turbulent shear flow. *Phys Fluids* 16:457
- Panton RL (1992) Scaling laws for the angular momentum of a completely turbulent Couette flow. *C R Acad Sci Paris Ser II* 315:1467
- Racina A, Kind M (2006) Specific power input and local micromixing times in turbulent Taylor–Couette flow. *Exp Fluids* 41:513
- Roberts PH (1965) Experiments on the stability of viscous flow between rotating cylinders. VI. Finite-amplitude experiments. *Proc. Roy. Soc. Lon.* 283:531 (in an appendix from Donnelly RJ, Schwarz KW)
- Schartman E, Ji H, Burin MJ (2009) Development of a Couette–Taylor flow device with active minimization of secondary circulation. *Rev Sci Inst* 80:1–024501
- Shankar PN, Kumar M (1994) Experimental determination of the kinetic viscosity of glycerol-water mixtures. *Proc R Soc Lond A* 444:573
- Smith GP, Townsend AA (1982) Turbulent Couette flow between concentric cylinders at large Taylor numbers. *J Fluid Mech* 123:7
- Taylor GI (1923) Stability of a viscous liquid contained between two rotating cylinders. *Phil Trans R Soc Lond A* 223:289
- Taylor GI (1935) Distribution of velocity and temperature between concentric rotating cylinders. *Proc R Soc Lond A* 151:494
- Taylor GI (1936) Fluid friction between rotating cylinders. I. Torque measurements. *Proc R Soc Lond A* 157:546
- Tong P et al (1990) Anisotropy in turbulent drag reduction. *Phys Rev Lett* 65:2780
- Wendt F (1933) Turbulente Strömungen zwischen zwei rotierenden konaxialen zylindern. *Ing Arch* 4:577